V International Conference on Simulation for Additive Manufacturing
Sim-AM 2025
F. Auricchio, M. Carraturo and S. Morganti (Eds)

FROM COMPUTED TOMOGRAPHY TO FINITE ELEMENT ANALYSIS: MAPPING POROSITY IN METAL ADDITIVE MANUFACTURING

L.M. CACHO[*], D.M. NETO[*], M.A. NETO[*] AND M.T. VIEIRA[*]

[*] Centre for Mechanical Engineering Materials and Processes (CEMMPRE)
Department of Mechanical Engineering, Universidade de Coimbra
Polo II, Rua Luís Reis Santos, 3030-788 Coimbra, Portugal
e-mail: luis.cacho@dem.uc.pt, www.uc.pt/cemmpre/

Key words: Multi-scale, Finite Element Analysis, Mapping of Porosity, Metal Additive Manufacturing (MAM), X-Ray Computed Tomography

Abstract. The present study aims to assess the accuracy of the mapping procedure used to transfer the porosity from the X-ray computer tomography (μXCT) images to the finite element mesh used in the numerical analysis. The uniaxial tensile specimen of stainless steel 316L obtained by material extrusion (MEX) was selected to evaluate the mapping procedure. The first step comprises the 3D representation of the specimen using a mesh composed by tetrahedral finite elements, where the internal porosity is defined in each element by the void volume fraction. The second step is the mapping of the porosity from this mesh to the mesh used in the numerical analysis, which is composed by hexahedral finite elements. The impact of the mesh size on the obtained porosity level was studied, considering different meshes in both steps, namely element size ranging between 0.019 and 0.5 mm in the donor tetrahedral mesh and element size ranging between 0.1 and 0.5 mm in the receiver hexahedral mesh. The results highlight the correlation between mesh size and volume fraction of porosity assigned locally.

1 INTRODUCTION

Structural Finite Element Analysis (FEA) is a state-of-the-art technique commonly used to design engineering components and to study the mechanical behaviour. FEA relies on the continuum and homogeneity assumptions [1]. However, multi-phase heterogeneous microstructures, are increasingly common in engineering, such as in metal Additive Manufacturing (AM) processes, which report multi-phase microstructures with stochastic porosity [2]. Another example is the fibre-reinforced polymer composites, where the distribution, shape and orientation of fibres influence the final mechanical behaviour of moulded objects [3].

Homogenization techniques have been used to study the impact of microstructure constituents on the part-scale macro mechanical behaviour of objects. The homogenization schemes calculate the effective properties of a volume with specific constituents, and these properties are attributed to the FEA structural mesh elements. Hu et al. [3] used the Digimat-MAP module to map the glass fibre orientation within the thermoplastic matrix between two different numerical analyses. The fibre orientation obtained from the simulation of the injection-moulded composite wheel was transferred to the Abaqus software to perform an

impact analysis. In a separate study, but using the same mapping procedure, they performed a similar FEA to assess the impact of residual stresses generated during the moulding process [4]. The mapping method used an extrapolation of the data from the element integration points to the element nodes, followed by the transfer to the integration points of the structural mesh (integration point/node to integration point).

The mapping of data is not limited to the connection between different numerical analyses. Cacho et al. [5] used the X-ray computer tomography (μXCT) non-destructive metrology analysis to detect porosity on a metal AM-processed specimen. Then, they transferred the porosity to the structural mesh to assess the mechanical behaviour of the specimen, considering all the porosity detected. The mapping was performed between dissimilar meshes using the Element to Integration Point (Ele2Int) method available in the Digimat-MAP module. Other researchers also used dissimilar meshes to map damage [6]. However, the mapping of data is highly sensitive to the mesh size, affecting the accuracy of the predicted structural behaviour. Hence, it is crucial to guarantee the accuracy of the mapping strategy.

The objective of this study is to assess the impact of mesh size on the mapping of porosity between dissimilar meshes using the Ele2Int method. The methodology for the two steps required to map porosity between the μXCT and the structural mesh will be presented and the conservation of porosity will be analysed. The parameters used to process the metal specimen and to acquire the images using X-ray are available in the authors previous publication [5].

2 METHODOLOGY

2.1 Sample Preparation

As mentioned previously, the processing parameters of the metal specimen used in this study are reported in [5], as well as the micro μXCT non-destructive analysis. The only difference is the volume analyzed in the μXCT. The reverse-engineered 3D object used in this study comprised only the gauge section of the tensile specimen. The total length of the specimen considered was approximately 33 mm.

2.2 Mapping of Porosity

The mapping strategy presented in this paper is part of a methodology used to assess the impact of porosity on the mechanical behaviour of metal AM components using a multi-scale FEA [5]. The methodology uses the interaction between three software packages: Volume Graphics (VG), Digimat, and Ansys. In the present work, only the procedure concerning the mapping of porosity will be studied. The mapping of porosity used by Cacho et al. [5] contains two different steps, occurring on two independent software packages: VG (version 2025.1) and Digimat-MAP (version 2022.2). The objective of this study is to assess the conservation of porosity volume during the mapping procedure using different meshes.

2.2.1 Mapping of porosity in the Donor Mesh – Step 1

Step 1 of the strategy to map porosity is graphically described in Figure 1 a). After 3D object reconstruction, the VG software is used to perform the new porosity analysis. The volume is defined by the specimen's outer surface. Consequently, the volume is discretized using tetrahedral elements, selecting the desired maximum and minimum element size. Then, the finite elements describing the specimen's volume are superposed onto the pore analysis, mapping the porosity into the integration points. The results are a Donor Mesh (DM) and a data

file (.csv) containing volume fraction of porosity assigned to each tetrahedral element. The superposition of the DM to the pore analysis is illustrated in Figure 1 b). The pores lose their geometrical identities and are represented by an element or a cluster of elements with an associated volume fraction.

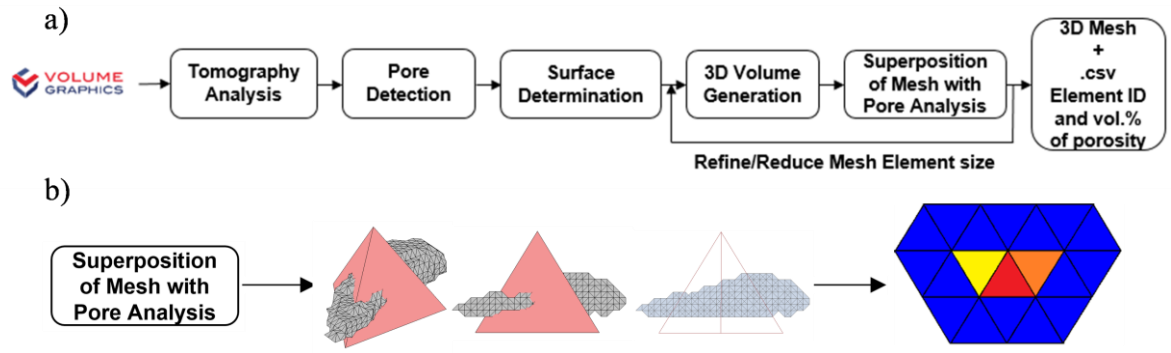

Figure 1: a) Overview of the step required for the mapping of porosity from the µXCT analysis to the DM. b) Transfer of porosity volume into finite mesh volume fraction.

To analyze the conservation of porosity during the mapping between dissimilar meshes, five linear tetrahedral (1 integration point) DM were created, which are listed in Table 1.

Table 1: Maximum and minimum element size used in the donor mesh to discretize the geometry.

Generated Donor Meshes: Element Size (mm)									
DM-1		DM-2		DM-3		DM-4		DM-5	
Máx.	Min.	Máx.	Min.	Máx.	Min.	Máx.	Min.	Máx.	Min.
0.1	0.1	0.3	0.3	0.5	0.2	1	0.1	1	0.0019

2.2.2 Mapping of Porosity from Donor to the Receiver Mesh – Step 2

The step 2 of the procedure for mapping porosity between meshes is illustrated in Figure 2 a). Using the Digimat- MAP (version 2022.2) module, information between different meshes can be exchanged. Three inputs are needed to perform the mapping: the DM and the respective data file containing element ID and volume fraction of porosity generated in VG (see Figure 1 a)), and the Receiver Mesh (RM) generated in ANSYS to discretize the receiver geometry. After uploading the two different meshes, a geometrical superposition must be done. It is crucial that both meshes occupy the same corresponding spatial position. Regarding porosity, Digimat software manual recommends the use of two different methods: integration point to node of the DM to the integration point of RM and element of DM to integration point of RM (Ele2Int). The Ele2Int method is schematically represented in Figure 2 b). After the superposition of the volumes, the tetrahedral element with a volume fraction of porosity will directly transfer the volume fraction to the hexahedral integration point (without shape function interpolation).

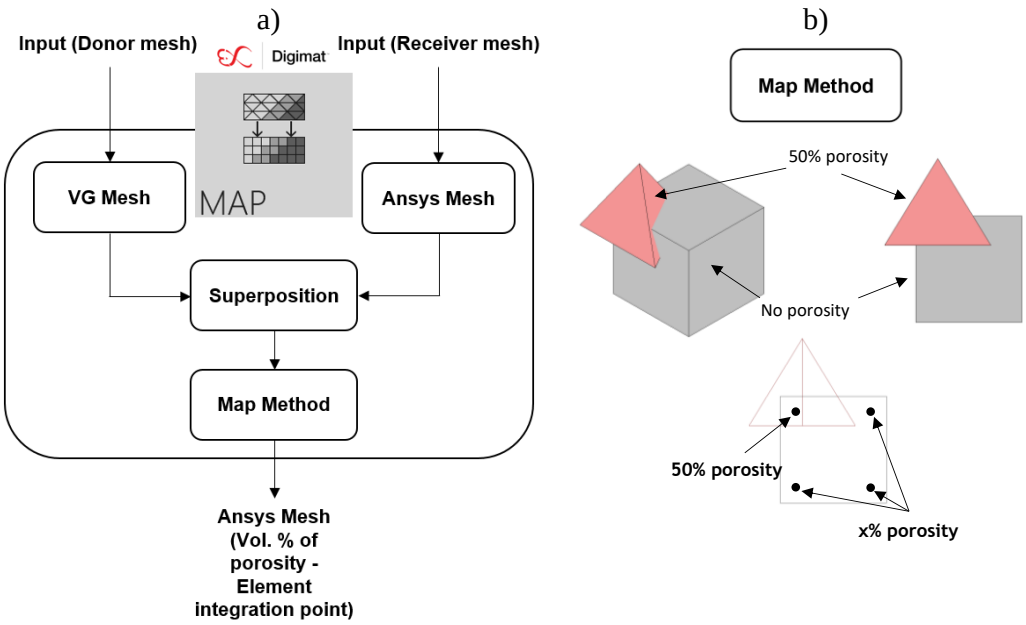

Figure 2: a) Overview of the step required to map the porosity between the DM and RM. b) Transfer of porosity volume fraction between dissimilar meshes using Ele2Int method.

A receiving geometry was created and discretized with three different regular hexahedral linear mesh elements (8 integration points). Since the specimen presents an irregular distribution of width and thickness through its length, it was necessary to create a geometry that would encompass all the donor geometries. The geometry dimensions and the element size are presented in Table 2. These three meshes were created to study the impact of mesh size on the conservation porosity volume between dissimilar meshes.

Table 2: Dimensions of the generated receiver geometry and respective regular hexahedral mesh elements used to discretize the three different RM.

Generated Receiver Geometry and Meshes (mm)									
	RM-A			RM-B			RM-C		
Receiver Geometry	L	H	T	L	H	T	L	H	T
	33	6.3	2.1	33	6.3	2.1	33	6.3	2.1
Subdivisions	330	63	21	165	30	10	66	14	5
Element size	0.1	0.1	0.1	0.2	0.21	0.21	0.5	0.45	0.42

3 RESULTS AND DISCUSSION

This section discusses the results related to µXCT porosity analysis, DM generation, and the preliminary mapping onto the DM, as well as the mapping between dissimilar meshes using the Ele2Int method. Ultimately, several problems are identified, representing the probable causes of the variability in the final porosity volume. The metal specimen µXCT pore analysis is presented in the Figure 3. The measured total volume is 421.93 mm^3, while the pore volume is 6.69 mm^3 (1.59% of porosity). There are four distinct types of porosity detected in the µXCT, namely: inter-bead, lack of overlap between infill and perimeters, debinding and sinter pores. Inter-bead porosity is identified by its elongated shape in the printing direction [7]. This specific

scenario represents an alternate infill with a 45º angle to the loading direction [5]. In the µXCT analysis, pores are also regularly present in the zones connecting the infill to the perimeters, suggesting a lack of overlap [8]. The largest pore, with a volume of 2.18 mm^3, was produced by the increase in pressure during the thermal debinding cycle [9]. The trapped gas caused the delamination of layers with weak bonding. Indeed, the delamination of this pore occurred in the layers with inter-bead porosity. These types of pores are present in limited layers, suggesting a lack of material extrusion during a determined period. Other process pores are distributed randomly throughout the volume.

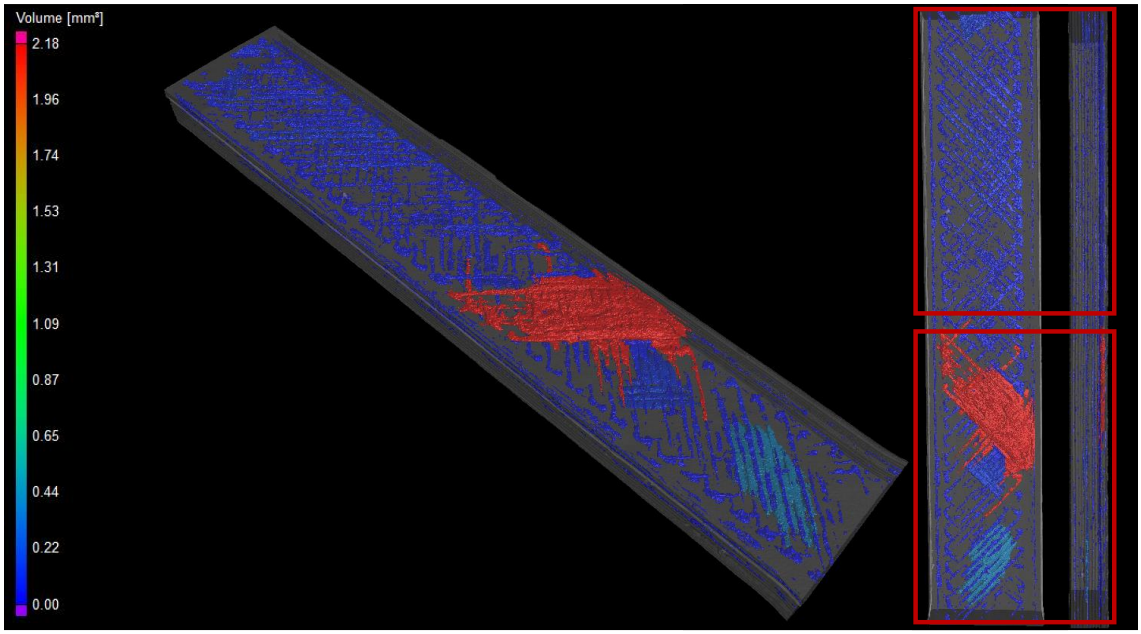

Figure 3: µXCT porosity analysis results: shape, size and distribution of porosity in the AM-processed metal specimen.

The maximum and minimum element size chosen to discretize the donor geometry directly affect the morphology of the meshed body and the volume fraction of porosity mapped onto the tetrahedral elements. Two different characteristics are identified immediately: lateral 3D object morphology, characteristics of the material extrusion process, and a significant surface defect. Usually, surface geometrical characteristics are lost during the discretization of a volume with coarser elements. Figure 4 shows how the maximum and minimum linear tetrahedral mesh element sizes, described in Table 1, affect the discretization of the cross-sectional image.

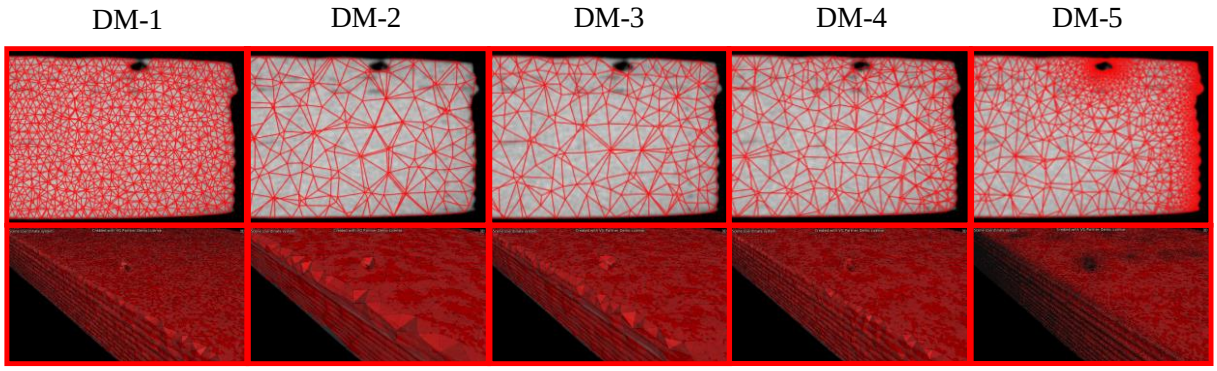

Figure 4: Impact of linear tetrahedral maximum and minimum element sizes in the discretization of the specimen cross section.

Coarser meshes were unable to geometrically define the surface defect and the 3D surface object morphology. Moreover, DM-2 and DM-3 failed to capture the whole surface volume near the hole. DM-5 was able to represent all the object features on the highlighted cross-section. The number of tetrahedral elements in DM-1, DM-2, DM-3, DM-4 and DM-5 is 1 851 868, 68 808, 102 622, 223 323 and 3 641 061, respectively. The element shape quality, evaluated by the ratio between the volume of the tetrahedron element and the volume of a regular tetrahedron with the same circumference is reported for all the DM in Figure 5. The higher the factor, the closer the element is to the regular shape. DM1 reported that 50% of the elements had an element shape quality of 0.84 or more. In average, the elements generated in DM2, DM3, DM 4 and DM5 had a ratio of 0.77, 0.75, 0.76 and 0.79, respectively. The generation of more distorted tetrahedrons was regularly seen when the discretization was performed with coarser element sizes.

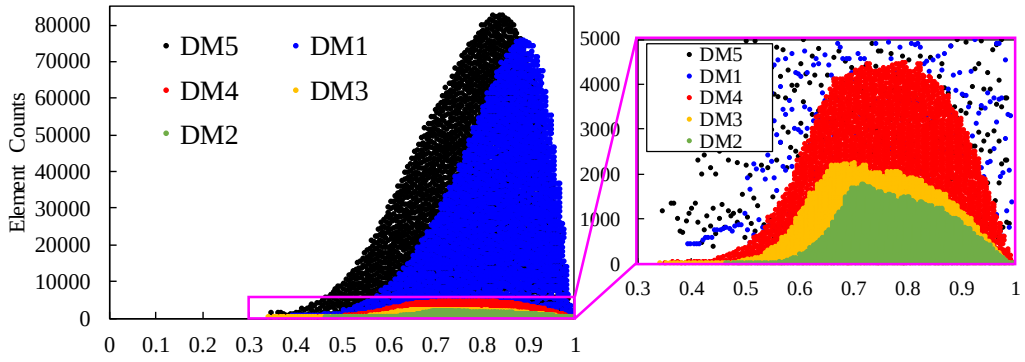

Figure 5: Element shape quality: ratio between the volume of the tetrahedron element and the volume of a regular tetrahedron with the same circumference.

The volume fraction of porosity associated with each element is affected by maximum and minimum element size. Coarser elements will be superposed onto the detected porosity (Figure 4), affecting the volume fraction of porosity of tetrahedral elements after preliminary mapping. The distribution of porosity on the different DM is presented in Figure 6. Discretizing the specimen with coarser elements redistributes the porosity volume fraction to the surface mesh, as evident in DM-2, DM-3 and DM-4. Moreover, the maximum volume fraction of porosity reported to DM-2 was 90.65%, while all the other 4 meshes reported a maximum volume fraction of 100%. Note that this issue concerns only the mapping of porosity, not the assessment

of effective properties with homogenization.

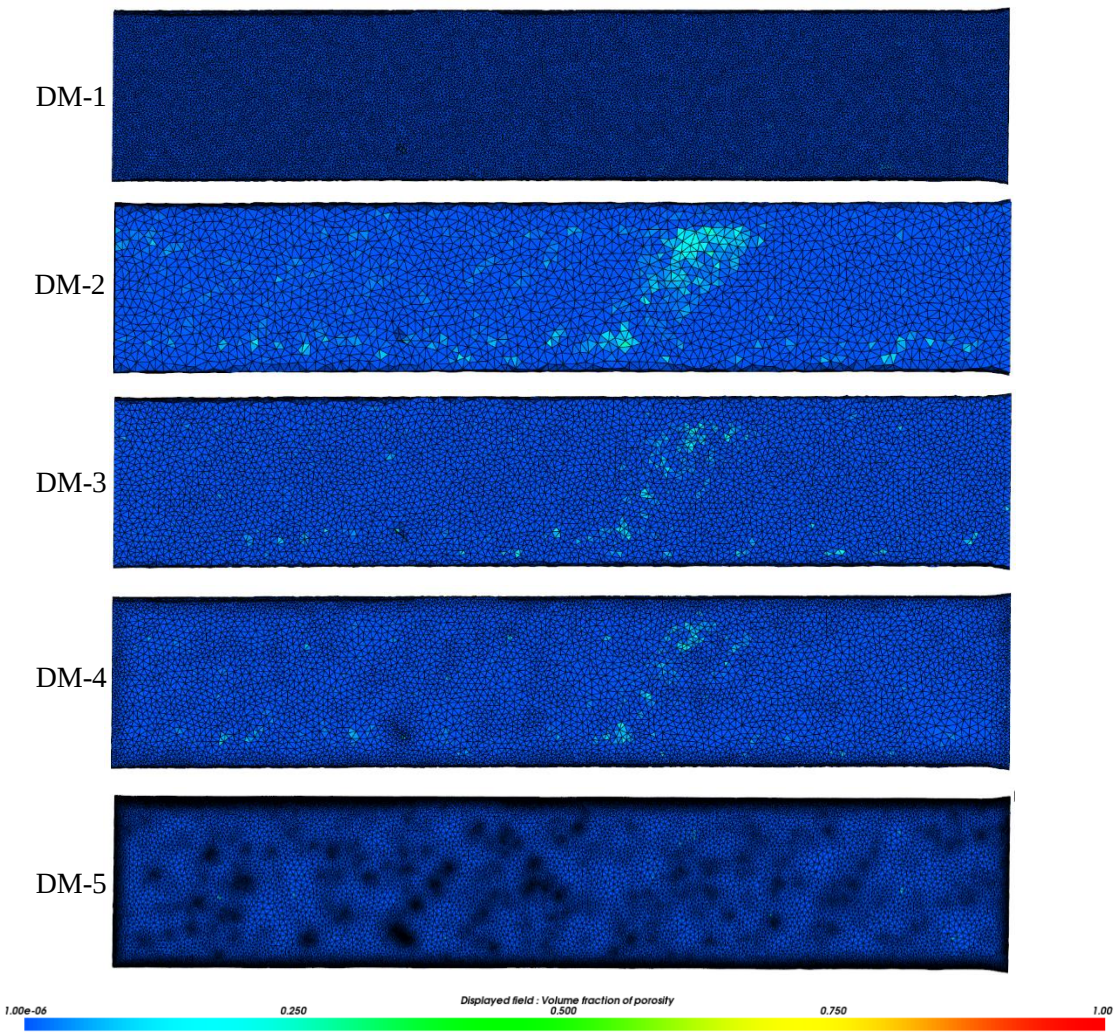

Figure 6: Impact of the linear tetrahedral element sizes in the distribution of volume fraction of porosity on the five different DM.

To study the conservation of volume of porosity during the mapping of dissimilar meshes, receiver geometries were created (see Table 2). The paralelepipedal geometry had a volume of 436.59 mm^3. The number of elements in the mesh RM-A, RM-B and RM-C is 436 590, 49 500 and 4 620, respectively. Notice that the donor and receiver geometries can have different sizes, as a large DM can be mapped into a smaller RM. The irregular width and thickness of the specimen through the length led to the generation of a receiver geometry with a larger volume. This was preferred to avoid large parts of DM not being superposed into RM, nevertheless, it was assumed that the difference in volume is negligible.

The effective volume of porosity of the RM was assessed using the finite element volume and the average volume fraction of each element. Since the donor and receiver geometry volumes are different, this induces a small deviation in the final calculated porosity. The final volume of pores was calculated for all the mapped cases and is reported in Table 3. The error was calculated by dividing the difference from the initial and final porosity volume by the final porosity volume.

Table 3: Results of the final volume of porosity after mapping between dissimilar messes.

Mapped Porosity								
From	DM-1	DM-1	DM-1	DM-2	DM-2	DM-2	DM-3	DM-3
To	RM-A	RM-B	RM-C	RM-A	RM-B	RM-C	RM-A	RM-B
Final Porosity Volume (mm^3)	6.66	6.88	5.1	6.70	6.69	6.65	6.68	6.71
Error (%)	-0.402	2.874	-23.71	0.107	0.001	-0.534	-0.211	0.233

From	DM-3	DM-4	DM-4	DM-4	DM-5	DM-5	DM-5
To	RM-C	RM-A	RM-B	RM-C	RM-A	RM-B	RM-C
Final Porosity Volume (mm^3)	6.85	6.68	6.71	6.64	6.69	6.82	5.81
Error (%)	2.404	-0.089	0.369	-0.730	0.004	1.884	-13.09

Figure 7 a) presents the comparison between the calculated porosity volume and the experimentally measured in the µXCT analysis (represented by the red line). Two outcomes were clearly highlighted. The mapping between dissimilar meshes using the Ele2Int method reported a considerable loss in porosity volume in the DM-1 to RM-C and in DM-5 to RM-C cases, with volume losses of 23.71% and 13.09% respectively. Contrary to this tendency, three cases reported an increase in pore volume: namely, DM-1 to RM-B, DM-3 to RM-C and DM-5 to RM-B. The variation of the maximum volume fraction of porosity on the RM elements during the mapping between dissimilar meshes is represented in Figure 7 b). As expected, the tendency shows that coarser receiver meshes will have lower values of maximum porosity volume fraction. Despite that, only two cases reported an abrupt loss in effective volume of pores.

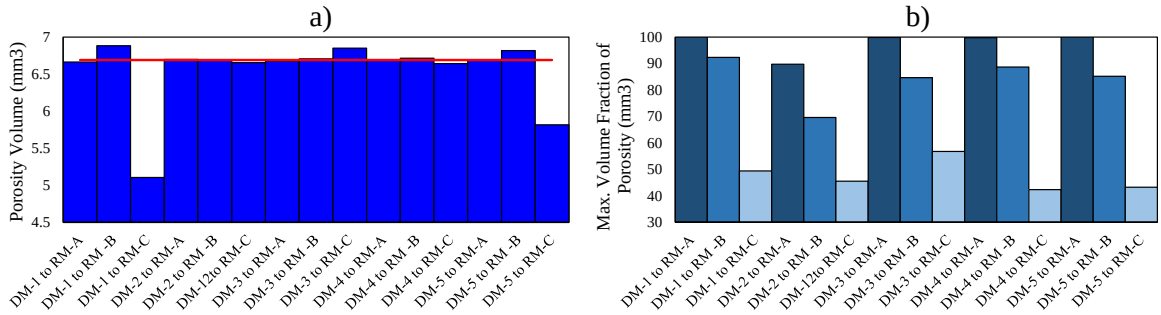

Figure 7: a) The global volume of porosity after mapping in all cases. b) Local maximum volume fraction of porosity in all cases studied.

Figure 8 presents the result of the porosity mapping between DM-5 and RM-A, RM-B and RM-C. The mapping from DM-5 to RM-A, which is the mapping between the meshes with the highest number of elements, reported an error of 0.004%. Similar to the preliminary mapping in step 1 (see DM-2, DM-3 and DM-4 in Figure 6), mapping porosity into coarser meshes projects the porosity volume fraction into a larger volume. The maximum averaged porosity recorded in the elements of RM-C when mapped from DM-5 was 43.21%. This case reported an overall loss of 13.09% of porosity.

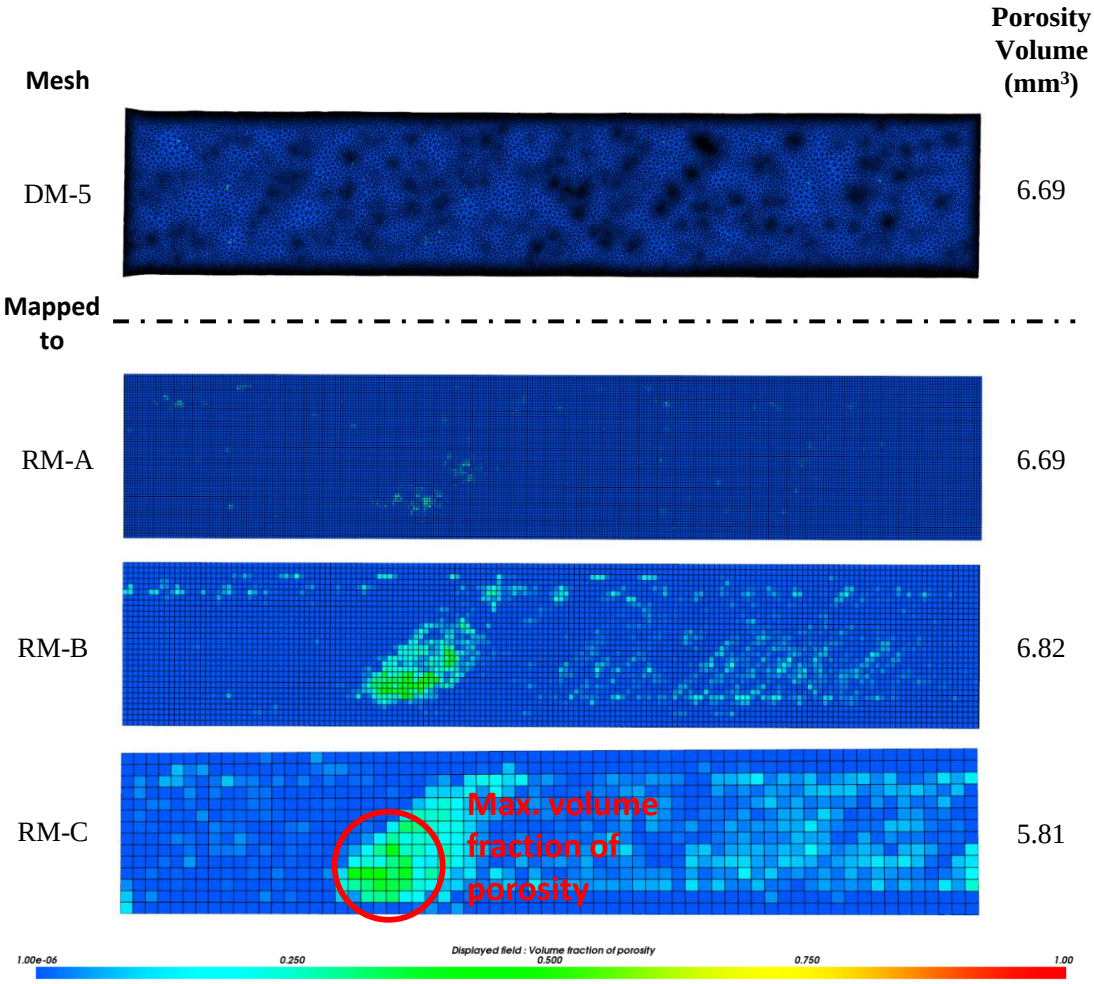

Figure 8: Mapping between the DM-5 onto all the three different RM: variation in final porosity volume and distribution over the RM surface.

The final volume of porosity mapped from the five different DMs to the most refined structural mesh (RM-A) is presented in Figure 9. The mapped total volume of porosity is identical in all cases, highlighting the importance of using a finer donor mesh. However, increasing the order of the hexahedral elements and consequently the number of integration points of the RM, the considerations might be different. Additionally, using an irregular hexahedral mesh refined locally may also help the conservation of porosity. Local refinements of RM would reduce the overall number of elements, while maintaining effectiveness in preserving porosity during the mapping of dissimilar meshes. The distribution of final porosity after mapping is differently affected by the selected DM, as shown in Figure 9. Only two cases (DM-1 to RM-A and DM-5 to RM-A.) show the mapped volume fraction of porosity at surface similar to the distribution of the respective DM (see Figure 6).

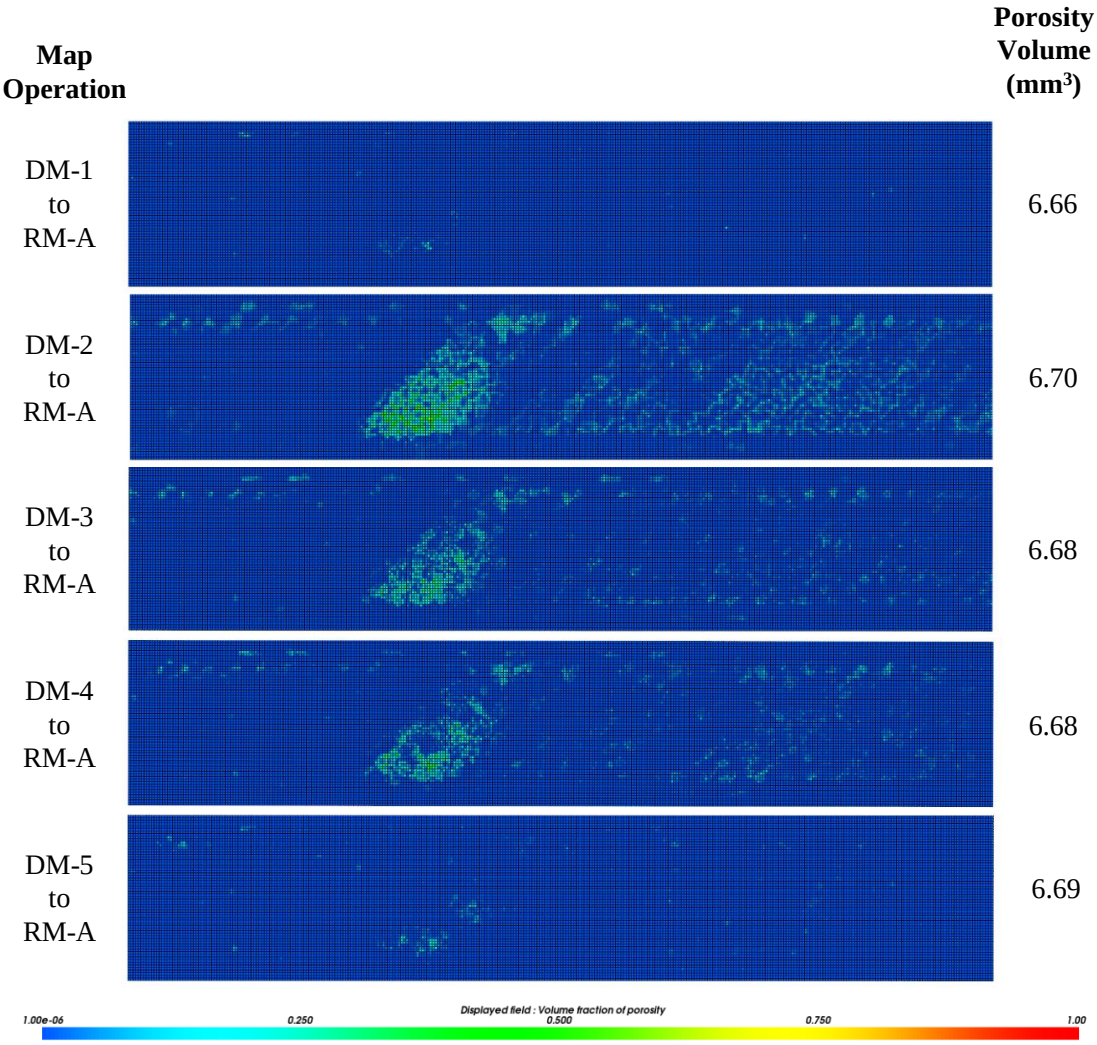

Figure 9: Mapping results of the cases where the porosity was mapped from all the five DM onto the RM-A.

Both the increase and the decrease of volume of porosity can occur after the mapping procedure between dissimilar meshes. When a fine DM is superposed onto a coarse RM, the porosity attributed to the integration points after mapping might fail to represent the porosity of that respective donor volume (Figure 10 a)). It is particularly important in DM with high gradients of volume fraction of porosity. Besides, highly distorted tetrahedral DM elements can contribute to the inconsistency of the final volume of porosity in a similar way (Figure 10 b)). Lastly, regular and consistently distributed processing defects (e.g., inter-bead porosity), can be mapped into the DM in a regular manner. Then, the elements of the DM with porosity volume fraction can be superposed regularly onto the RM integration points, leading to an increase in final volume, as shown in Figure 10 c). The opposite will result in a decrease in the final volume of pores.

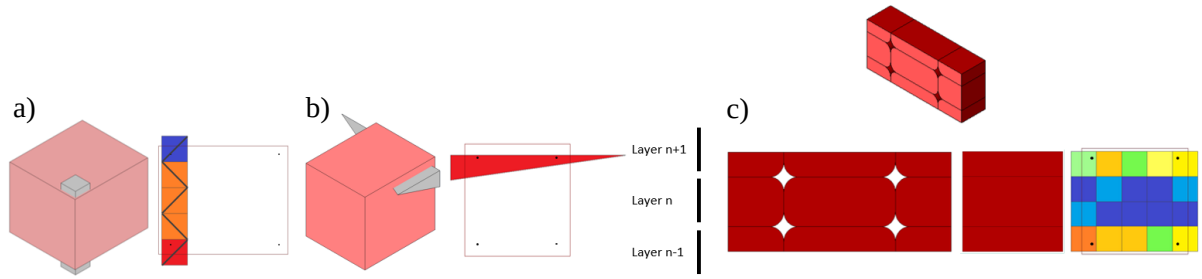

Figure 10: Probable causes that influence the final volume of porosity after mapping: a) mapping from a fine mesh into a largely coarser mesh; b) distorted DM elements; c) systematic superposition of process defects onto the RM element integration points.

4 CONCLUSIONS

The accuracy of the mapping method Ele2Int was evaluated in the present study, considering the mapping of the volume fraction from µXCT analysis to the FEA. Four types of porosity were identified in the non-destructive analysis of the specimen processed by AM: inter-bead, delamination, lack of overlap and random diffuse porosity. Using the Ele2Int method with dissimilar meshes, the error of the mapped porosity volume ranged from -23.7% and 2.8%. The error of the mapping procedure is higher when mapping from finer Donor Meshes into coarser Receiver Meshes. The presence of distorted Donor Mesh elements also affect the conservation of porosity in a similar manner. The superposition of systematic regular porosity, originated due to process characteristics, onto the integration points of the Receiver Mesh, may also be a problem when mapping data between dissimilar meshes. In conclusion, considering the final volume of porosity, the best accuracy is obtained when mapping from finer Donor Meshes to finer Receiver Meshes. If a coarser Donor Mesh is used and the Receiver Mesh cannot be refined, the mesh should have around the same element size.

ANKOWLEDGEMENTS

This work was carried out within the framework of the “Agendas para a Inovação Empresarial” (Project no 49, acronym “INOV.AM”, with reference PRR/49/INOV.AM/EE, operation code 02/C05 i01.01/2022.PC644865234-00000004), supported by the RRP Recovery and Resilience Plan and by the European Funds NextGeneration EU. http://www.recuperarportugal.gov.pt/. This research was sponsored by national funds through the FCT—Fundação para a Ciência e a Tecnologia, under the projects UID/00285—Centre for Mechanical Engineering, Materials and Processes, LA/P/0112/2020

REFERENCES

[1] P.F. Rodrigues, L. Cacho, D. Gatões, B. Alves, M.A. Neto, A. dos S. Paula, F.M.B. Fernandes, A.S. Ramos, M.T. Vieira, Embedded NiTi Strain Sensors in Additively Manufactured AlSi10Mg: Computational and Experimental Insights into Phase Transformation and Sensing Performance, Results Eng. 28 (2025) 107395. https://doi.org/10.1016/j.rineng.2025.107395.

[2] F.R. Cruz, N. Alves, T. Vieira, Direct additive manufacturing as spring of new tool steels, J. Mater. Res. Technol. 26 (2023) 5450–5461. https://doi.org/10.1016/j.jmrt.2023.08.176.

[3] D. Hu, Y. Shan, T. He, X. Liu, X. Wan, Research on simulation method of impact resistance of composite wheels made of long glass fiber reinforced thermoplastic introducing anisotropic property, Compos. Struct. 223 (2019) 110965.

https://doi.org/10.1016/j.compstruct.2019.110965.
[4] D. Hu, Y. Shan, T. He, X. Liu, Analysis on effect of injection residual stress on impact resistance of composite wheel made of long glass fiber reinforced thermoplastic, Int. J. Crashworthiness. 26 (2021) 515–525. https://doi.org/10.1080/13588265.2020.1757583.
[5] L.M. Cacho, M.A. Neto, D.M. Neto, M.T. Vieira, Coupling μ-computed tomography and multi-scale modelling to assess the mechanical performance of material extrusion metal components, J. Mater. Res. Technol. 30 (2024) 3238–3250. https://doi.org/10.1016/j.jmrt.2024.04.065.
[6] R. Sachse, A.K. Pickett, P. Middendorf, Simulation of impact and residual strength of thick laminate composites, Compos. Part B Eng. 195 (2020) 108070. https://doi.org/10.1016/j.compositesb.2020.108070.
[7] A. Pellegrini, M.E. Palmieri, M.G. Guerra, Evaluation of anisotropic mechanical behaviour of 316L parts realized by metal fused filament fabrication using digital image correlation, Int. J. Adv. Manuf. Technol. 120 (2022) 7951–7965. https://doi.org/10.1007/s00170-022-09303-z.
[8] S. You, D. Jiang, F. Wang, F. Ning, Anisotropic sintering shrinkage behavior of stainless steel fabricated by extrusion-based metal additive manufacturing, J. Manuf. Process. 101 (2023) 1508–1520. https://doi.org/j.jmapro.2023.07.026.
[9] Z. Lotfizarei, A. Mostafapour, A. Barari, A. Jalili, A.E. Patterson, Overview of debinding methods for parts manufactured using powder material extrusion, Addit. Manuf. 61 (2023) 103335. https://doi.org/10.1016/j.addma.2022.103335.